Coupling Analysis of Probe Diffusion in High Molecular Weight Hydroxypropylcellulose

Kiril A. Streletzky and George D. J. Phillies*

Department of Physics, Worcester Polytechnic Institute, Worcester, Massachusetts 01609

Received: June 29, 1998; In Final Form: January 14, 1999

The coupling/scaling model of Ngai and Phillies [Ngai, K. L., Phillies, G. D. J. *J. Chem. Phys.* **1996**, *105*, 8385] is applied to light scattering spectra of mesoscopic probes in 1 MDa hydroxypropylcellulose (HPC): water. Spectra are bimodal. The coupling/scaling model works for one mode but not the other. Probes smaller than the hydrodynamic radius of the HPC show a two-stretched-exponential relaxation: The slow mode follows coupling/scaling predictions; the fast mode does not. Probes whose diameters are comparable to or larger than the radius of gyration have spectra composed of a fast, stretched-exponential mode that follows coupling/scaling, and a slow, pure-exponential mode not described by coupling/scaling. Interpretations of the success or failure of the coupling/scaling model for various modes and probes are advanced, based on relationships between the observed and assumed spectral line shapes, and on the absolute time scale of each relaxation.

Introduction

The mechanism of polymer dynamics in dilute and concentrated solution remains a subject of substantial interest. Many theoretical approaches[1−4] have been developed to treat polymers in solutions and melts, but the nature of polymer dynamics remains unclear. A major test of treatments of polymer dynamics is the dependence of transport coefficients on solution properties. Phenomenologically, the self-diffusion coefficient D_s depends on concentration c and molecular weight of the polymer M via a stretched exponential[3,5−8]

$$D_s = D_{s0} \exp(-\alpha c^{\nu} M^{\gamma}) \quad (1)$$

The zero-shear solution viscosity over a wide range of c is described well by another stretched exponential (ref 9 and references therein)

$$\eta = \eta_0 \exp(a c^{\nu} M^{\gamma}) \quad (2)$$

Here α and a are scaling prefactors, ν and γ are scaling exponents different for each system and property, and D_{s0} and η_0 are zero-concentration limits of D_s and η, respectively. Experimental data show[9] that, at very high c and M, η often changes its concentration and molecular weight dependence to a power law in c and M. The transition of η from stretched-exponential to power-law behavior has been referred to as the solution-like−melt-like transition.[9,10] The hydrodynamic scaling model of Phillies[3,5] directly derives eq 1 and implies a solution−melt-like transition.[5,9,10] Substantial experimental support for the hydrodynamic scaling model has been reported (refs 3, 5, 7, 8−12 and references therein).

Photon correlation spectroscopy determines the line shape $S(q,t)$ of the light scattering spectrum. Numerous studies of gelling systems[13−15] specifically address the spectral line shape. Many studies (ref 15 and references therein) find that $S(q,t)$ of gelling systems in the sol state is well described by a single stretched exponential (Kohlrausch−Williams−Watts (KWW) function) or by a sum of two KWW functions. In proximity to the gel point, $S(q,t)$ of a gelling system shows[15−17] a two-mode relaxation: a pure exponential initial decay and a slower power-law decay. $S(q,t)$ of polymer solutions[6,18,19] and of probes in polymer solutions[11,20−22] are similar to $S(q,t)$ of gelling systems; they are well represented by KWW functions. From a variety of experimental methods, other characteristic relaxations of polymer systems, such as the translational relaxation function measured by fluorescence recovery after photobleaching[23] and the spin−echo attenuation function,[24] are also represented well by KWW functions.

The coupling model of Ngai et al.[4,25] directly addresses the relaxation of complex systems and considers the relaxation spectrum's line shape. In this model, relaxations in complex systems are considered to be the "cooperative process of motions coupled together by interactions."[25] In the coupling model the relaxation line shape is a KWW function. This model is consistent[4] with eqs 1 and 2. According to this model, the dynamic constraints (degree of coupling) between the polymer chains control relaxation rates. These constraints vary in strength as polymer concentration changes. In dilute solutions, there is almost no coupling; the degree of coupling increases with increasing concentration.[4,6,25,26] There is considerable experimental support for the Ngai coupling model for polymer dynamics.[4,6,25−30]

An approach to understanding polymer dynamics is to study the diffusion of mesoscopic probes in polymer solutions. If the probes are dilute and scatter most of the light, the scattering spectrum of a polymer/probe/solvent ternary system reveals probe diffusion through an unseen matrix. In many polymer solutions, the self-diffusion coefficient D_p of probes can be[5,31] inferred from the light scattering spectrum. In almost all instances, $D_p(c)$ obeys eq 1. Ngai[32] emphasizes that probe diffusion in polymer solutions "should be well described by the coupling model, if that model is applicable at all."

Ngai and Phillies[32] recently presented a coupling/scaling analysis of polymer solutions that incorporates phenomenological predictions for D_p, η, and the line shape. Ngai and Phillies[32] derived equations for the degree of coupling as a function of η or $S(q,t)$ from probe diffusion. They demonstrated[32] that the

* To whom communications may be addressed. E-mail: phillies@wpi.wpi.edu (Internet).

10.1021/jp982804v CCC: $18.00
Published on Web 03/02/1999

degrees of coupling, independently calculated from the experimental time, concentration, or angular dependences of $S(q,t)$, or from the concentration dependence of η, are mutually consistent for the data of ref 20 on probes in solutions of 300 kDa hydroxypropylcellulose (HPC).

Reference 21 studied probes in 1 MDa HPC solutions at polymer concentrations $0 \leq c \leq 7$ g/L, using polystyrene latex sphere (PSL) probes of 8 different nominal diameters ($14 \leq d \leq 455$ nm). Most experiments in ref 21 used 90° scattering (with $q = 2.30 \times 10^5$ cm^{-1}), but the q dependence of $S(q,t)$ was studied extensively. This paper applies the Ngai−Phillies coupling/scaling model[32] to the new data of ref 21 on probe diffusion.

Ref 21 studied dilute, strongly scattering probes in solutions of a weakly scattering polymer. It is essential to emphasize that the observed relaxations correspond to probe diffusion, not to polymer concentration fluctuations. As a control, we compared under identical operating conditions spectra of these probes in polymer solutions and spectra of probe-free polymer solutions. Spectra of probe-free polymer solutions are far weaker than spectra of polymer solutions containing probes. For probes with $d \geq 50$ nm, matrix scattering at all t is less than 1% of probe scattering. For smaller ($d < 50$ nm) probes at high HPC concentration, polymer scattering is more substantial, but probes scatter much more light than polymer does. For most probes and HPC concentrations, $S(q,0)$ of a probe-free polymer solution is ≤1% of $S(q,0)$ of the corresponding probe:polymer solution. In the worst case (smallest spheres, highest HPC concentration) $S(q,0)$ of the polymer solution is <4% of $S(q,0)$ of the probe:polymer solution. The amplitude ratio depends on the time scale. $S(q,t)$ of a probe:polymer sample decays somewhat faster than does $S(q,t)$ of a probe-free polymer sample. To confirm that polymer scattering did not influence our spectral analysis, we measured spectra of probe:polymer mixtures and probe-free polymer solutions under the same conditions, subtracted (at the field correlation level) the polymer spectrum from the probe:polymer spectrum, and analyzed the difference spectrum. For all HPC concentrations, at the time scales covered by this study, the difference spectrum is fit by the same function and parameters that we obtained without subtraction. The effect of spectral subtraction on the fitting parameters is comparable to the experimental error in those parameters. Polymer scattering, therefore, does not influence probe spectra of ref 21 significantly. Polymer modes, while not negligible on all time scales, did not perturb ref 21's line shape parameters significantly. Reference 21's spectra thus reflect high-accuracy probe motions in an unseen polymer matrix.

Further sections discuss line shape analysis, describe our results and data interpretation, and compare our findings with the literature. A discussion with conclusions closes the paper.

Line Shape Analysis

We analyzed spectra by fitting them to specific functional forms. This section explains which forms were used in ref 21. The intensity−intensity correlation function $g^{(2)}(q,t)$ is related to the field-correlation function $g^{(1)}(q,t)$ via

$$g^{(2)}(q,t) = S(q,t) - B = A(g^{(1)}(q,t))^2 \qquad (3)$$

where A is the scattering amplitude, B is the baseline (the time-independent part of the spectrum), and $q = (4\pi n/\lambda)\sin(\theta/2)$ is the scattering vector. In ref 21 we tried different forms of $g^{(1)}(q,t)$ to see which one best describes $g^{(2)}(q,t)$; we minimized $[g^{(2)}(q,t) - S(q,t)]^2/[S(q,t)]^2$.

For all probe diameters and $c > 0$ g/L, we found[21] clear bimodal spectra. The field correlation function fits well to a sum of two stretched exponentials, namely

$$g^{(1)}(q,t) = (1 - A_f)\exp(-\theta t^{\beta_t}) + A_f \exp(-\theta_f t^{\beta_{ft}}) \qquad (4)$$

where β_t and β_{ft} are stretching exponents, and θ and θ_f are the decay pseudorates, of the slow and fast modes, respectively. A_f is the amplitude fraction of the fast mode. Equation 4 can alternatively be written

$$g^{(1)}(q,t) = A_f \exp\left(-\left(\frac{t}{\tau_f}\right)^{\beta_{ft}}\right) + (1 - A_f)\exp\left(-\left(\frac{t}{\tau}\right)^{\beta_t}\right) \qquad (5)$$

where $\tau = \theta^{-1/\beta_t}$ and $\tau_f = \theta_f^{-1/\beta}$ are the time scales, with units time[1]. As discussed ff. eq 13, ref 21 demonstrated that θ, not τ^{-1}, is the physically fundamental transport coefficient.

Spectra of smaller probes are obviously bimodal, as revealed by the presence of two shoulders in plots of ln S(q,t) against ln t. Since the first shoulder was to good aproximation a stretched exponential in t, it was natural to suppose that the double relaxation was a sum of two stretched exponentials in t, as we confirmed numerically. Fitting the large-probe spectra with the same or similar functional form was a natural extension, though for larger probes the two relaxations are less well separated, requiring care in the fitting procedures,

While all probes produced clear bimodal spectra, we saw different diffusive behaviors for small and for large probes. For large probes (diameter $d > 67$ nm), spectra fit to eq 4 with $\beta = 1$. For small probes ($d < 67$ nm), spectra fit to eq 4 with β as a free parameter; we found $\beta < 1$. Spectra of 67 nm probes were analyzed using both $\beta = 1$ and β as a free parameter. The relevant characteristic length separating "small" and "large" probes is the characteristic size of an entire polymer chain. Small probes have $d < R_h$, R_h being the polymer hydrodynamic radius. Large probes have $d \geq R_g$, R_g being the polymer radius of gyration.

For all spheres, the fast mode has features[21] characteristic of chain internal motions. In contrast, the slow modes differ between the large- and the small-probe regimes. The slow mode of large probes is diffusive. The slow mode of small probes shows many features characteristic of diffusive behavior but also shows signs of coupling to chain internal motion.

The analysis of ref 21 built on earlier studies[11,20,33,34] of probe diffusion in HPC:water. Studies by Brown and Rymden[33] and Mustafa and Russo[34] on PSL:HPC:water both found probe spectra with bimodal relaxations. Brown and Rymden[33] used multiexponential analysis of $g^{(1)}(q,t)$ for probes in 800 kDa HPC. Mustafa and Russo[34] used multiexponential analysis and two different Laplace inversion methods for probes in 300 kDa HPC. References 33 and 34 agree: two relaxation modes were present in each spectrum.

Phillies et al.'s[11] original work on the PSL:HPC:water system studied spherical probes in solutions of HPC with nominal molar masses of 60, 100, 300, and 1000 kDa. Phillies et al.[11] successfully fit measured spectra using

$$g^{(1)}(q,t) = \exp(-\theta t^{\beta}) = \exp\left(-\left(\frac{t}{\tau}\right)^{\beta}\right) \qquad (6)$$

For probes in solutions of 60 and 100 kDa HPC, spectra were nearly purely exponential, with $\beta \in 0.85-1$. Probes in 300 kDa

HPC had $\beta \in 0.65-1$. For probes in 1 MDa HPC, Phillies et al.[11] showed that $g^{(1)}(q,t)$ is described adequately by eq 6, but noted a possible additional slow mode. The consequent study of ref 20 found that in 300 kDa HPC $g^{(1)}(t)$ follows eq 6 at low concentrations ($c < 10$ g/L), but at higher concentrations a second exponential mode becomes obvious so that $g^{(1)}(t)$ follows

$$g^{(1)}(q,t) = A_e \exp(-\theta_e t) + (1 - A_e) \exp(-\theta t^{\beta}) \qquad (7)$$

Equation 7 is due to Nystrom et al.,[28] based on the Ngai's coupling model.[4] The fast decay was very weak, $0.01 \leq A_e \leq 0.04$.

The discrepancy in the spectral line shape interpretation between refs 11 and 20 arose because ref 11 followed $g^{(2)}(q,t)/g^{(2)}(q,0)$ for a 10- to 20-fold decay, while ref 20 followed a 40- to 80-fold decay of $g^{(2)}(q,t)/g^{(2)}(q,0)$. By comparison, spectra of ref 21 examined below cover a 100- to 5000-fold decay of $g^{(2)}(q,t)/g^{(2)}(q,0)$. This advance allows accurate line shape analysis, revealing a bimodal relaxation, the second (slow) mode being dominant for $g^{(2)}(q,t)/g^{(2)}(q,0) < 0.05$. In addition to studying spectra at longer times than prior works, ref 21 also obtained spectra at the smallest attainable times. Covering a very wide time range produced a superior description of the total relaxation.

The Coupling-Scaling Model

The coupling model of Ngai[4,25-27] is a general treatment for "the dynamics of constrained, interacting systems."[32] The general derivation of the coupling model for complex systems from first principles is not known yet. However, for several simple systems with idealized Hamiltonians,[30,35,36] the theoretical simulations based on the classical mechanics of systems exhibiting chaos produced the basic predictions of the coupling model. The problem of relaxation in the interacting arrays of coupled nonlinear oscillators[35] and the classical Fermi acceleration problem with introduced nonlinearity[36] are just two most recent examples of theoretical models that directly yield the predictions of the coupling model.

The model treats a system as a combination of "basic units" that interact nonlinearly with each other. The coupling model recognizes two time regimes, separated by a crossover time t_c. At short times ($t < t_c$) "basic units" relax independently; their relaxation is characterized by a time correlation function

$$\phi(t) = \exp(-t/\tau_0) \qquad t < t_c \qquad (8)$$

τ_0 is the characteristic time for unconstrained relaxation. At $t > t_c$, cooperative constrains between "basic units" come into play. $\phi(t)$ then depends on the degree n ($0 \leq n < 1$) of coupling between basic units, so that

$$\phi(t) = \exp(-(t/\tau)^{(1-n)}) \qquad t > t_c \qquad (9)$$

Here τ is the characteristic time for constrained relaxations. A continuity condition on $\phi(t)$ at $t = t_c$ gives

$$\tau = [t_c^{-n}\tau_0]^{1/1-n} \qquad (10)$$

For nondilute polymer systems, chain centers of mass can be considered to be "basic units". The coupling model does not specify which interactions (e.g., hydrodynamic, topological) create the cooperative constraints. The coupling model should describe the diffusion of mesoscopic probes through polymer solution well, because probe diffusion involves an averaged motion of neighboring chains.

The coupling model predicts several features of the phenomenologies of probe diffusion in polymer solutions[11,20,31] and of polymer self-diffusion.[24,28] First, one can identify $g^{(1)}(t)$ with $\phi(t)$, with a stretching exponent $\beta = 1 - n$. KWW functions describe relaxations in many polymer systems[6,11,18-20,31] as predicted by the coupling model. Second, Ngai and Phillies[32] demonstrate that the phenomenological dependence of β[11-13,18,31] on polymer concentration is generally consistent with coupling model predictions for $1 - n$. Third, the coupling model predicts[32] that the relaxation time τ of eq 6 follows

$$\tau \equiv \theta^{-1/\beta_q} \sim q^{-2/(1-n)} \qquad (11)$$

Indeed, for probes in 300 kDa HPC, and for the slow mode of probes in 1 MDa HPC, θ experimentally[11,20,31] follows $\theta \sim q^2$, so $\tau \sim q^{-2/\beta}$ as predicted by the coupling model.

Ngai and Phillies[32] developed arguments connecting the coupling model to eq 1. The coupling/scaling model gives a coupling parameter n_D, analogous to n, but calculated from the concentration dependence $D_s(c)$, namely

$$\beta_c \equiv 1 - n_D = \left[\frac{3\nu}{2} + \frac{(3\nu - 1)(\ln(D_s(c^*)) - \ln(D_s(c)))}{2\ln(c/c^*)}\right]^{-1} \qquad (12)$$

where c^* is a nominal overlap concentration, and ν from $R_g \sim M^{\nu}$ relates the radius of gyration R_g of a polymer to its molecular weight M. Equation 12 is most plausible for nondilute solutions, i.e., for $c \gtrsim 2c^*$.

Ngai and Phillies then connected θ, β, and τ of eq 6 with $D_s(c)$ of eq 12. If probe motion is diffusive, then $\beta = 1$ and

$$g^{(1)}(t) = \exp(-\Gamma t) = \exp(-D_s q^2 t) \qquad (13)$$

Here Γ is a true decay rate; $\Gamma = D_s q^2$. When $\beta \neq 1$, Ngai and Phillies[32] identified Γ with θ because Γ and θ depend in similar ways on external parameters. In particular, (1) the theoretical Γ is $\sim q^2$, while experimentally $\theta \sim q^2$; (2) $\Gamma \sim \eta^{-1}$ (Stokes-Einstein relation), while experimentally θ is approximately $\sim \eta^{-1}$. Ngai and Phillies therefore replaced D_s with θ in eq 12 and computed n_D. An alternative identification for a stretched exponential relaxation would be $D_s q^2 \rightarrow \tau^{-1}$.

Ngai and Phillies[32] also developed coupling/scaling arguments connecting the coupling model to eq 2 for η. They extracted a degree of coupling n_η from the concentration dependence of η via

$$\beta_\eta \equiv 1 - n_\eta = \left[\frac{3\nu}{2} + \frac{(3\nu - 1)(\ln(\eta(c)) - \ln(\eta(c^*)))}{2\ln(c/c^*)}\right]^{-1} \qquad (14)$$

Here n_η is the coupling parameter for shear viscosity.

Equations 6, 11, 12, and 14 provide four independent paths for obtaining the degree of coupling $n \equiv 1 - \beta$: (1) β_t from the t dependence of $g^{(1)}(t)$, (2) β_q from the q dependence of $g^{(1)}(t)$, (3) β_c from the concentration dependence of θ or τ^{-1}, and (4) β_η from the concentration dependence of η. Ngai and Phillies[32] used these paths for obtaining β to analyze experimental data[10,20] on probe diffusion in 300 kDa HPC solutions. They demonstrated that β_c (from eq 12 using either $D_p q^2 \rightarrow \tau^{-1}$ or $D_p q^2 \rightarrow \theta$), β_t from $g^{(1)}(t)$, and β_η from $\eta(c)$ agree with each other.

Now we consider how to apply the coupling/scaling model as developed by Ngai and Phillies[32] to new data of ref 21 on higher molecular weight ($M = 1 \times 10^6$) HPC. A simple repeat of ref 32's analysis is impossible, because the spectra of ref 21

have two relaxational modes, not one. The two modes appear to be very different in their physical nature. In particular, ref 21 proposed that the fast mode involves probe motions coupled to chain internal modes; the slow mode, especially for large probes, appears to reflect simple Brownian diffusion of the probes in the polymer matrix. Diffusion of large probes requires whole-chain center-of-mass motions, but simple diffusion of small probes can be accommodated by local chain motions. However, the spectra[21] are characterized by two decay rates (pseudorates if $\beta \neq 1$) θ and θ_f (or τ and τ_f), and two stretching parameters, β and β_f. Reference 21's spectra do not simply imply a single diffusion coefficient D_p that could be substituted in eq 12. The spectra of ref 21, and ref 21's interpretation of these modes may be given a rational physical interpretation in terms of Ngai's coupling model. Namely, one supposes that the system contains two independent groups of "basic units", each of which separately is described by the Ngai model and its extensions, as seen in eqs 8−14. The two groups of "basic units" are strongly coupled within each group but are very weakly coupled between groups. Physically, the "basic units" are modes of motion of the chains, such as center-of-mass motion and chain internal modes, and not two distinct chemical species or types of particles.

Here we analyze each mode separately by applying the coupling/scaling model to see which modes follow the predictions of the coupling model. From eqs 12−14 we obtain two sets of coupling coefficients: β_t and β_c for the slow mode and β_{ft} and β_{fc} for the fast mode. β_η is the same for each mode because it is calculated from $\eta(c)$, not $g^{(1)}(t)$. Even though we cannot simply apply the coupling/scaling model (eqs 12−14)[32] to the whole relaxation and must deal separately with each mode, we can compare β_t, β_c, β_{ft}, and β_{fc} to β_η to infer the coupling behavior for each mode. β_η is a key to these comparisons because it reflects the motion of complete chains, follows directly from coupling/scaling analysis[32] without auxiliary assumptions, and is a solution property unrelated to the probe radius.

To anticipate our results, some modes follow approximately the coupling/scaling model. The slow mode of small probes shows tolerable agreement with coupling/scaling, but the slow mode of large probes does not follow coupling/scaling predictions. The fast mode for small probes does not follow coupling/scaling predictions, but the fast mode of large probes is very successfully described by coupling/scaling. It is noteworthy that the two modes (small-probe slow mode and large-probe fast mode) that obey the coupling/scaling model occur on the same absolute time scale.

Coupling/Scaling Analysis of the Slow Mode

Figures 1 (small probes) and 2 (large probes) present a coupling/scaling analysis of the slow mode of $g^{(1)}(t)$, comparing β_t and β_c for the slow mode with β_η from the solution viscosity. Here: β_t was obtained from the time dependence of $g^1(t)$ using eq 4 ($\beta_t = 1$ for large spheres), β_c was obtained from $\theta(c)$ and eq 12, and β_η was obtained from $\eta(c)$[10] via eq 14. Equations 12 and 14 require a nominal overlap concentration c^*. From ref 10, $c^* = 1/[\eta]$ for 1 MDa HPC is 1.4 g/L. Equations 12 and 14 for β_c and β_η also require ν; we tried three values for ν, namely 0.5, 0.55, and 0.6. With increasing ν, β_c and β_η fall. The β_η and β_c calculated with a specific ν are denoted $\beta_{\eta,\nu}$ and $\beta_{c,\nu}$, respectively.

$\beta_{\eta,\nu}$ is the same on each figure, because it is calculated from the zero-shear viscosity η of the polymer solution and not from a probe property. Near c^*, $\beta_{\eta,\nu}$ is scattered because there is a numerical artifact; at c^* eq 14 approaches ln(1)/ln(1). As noted by ref 32, the applicability of eq 14 is less clear for $c < c^*$. For $c > c^*$, $\beta_{\eta,\nu}$ decreases smoothly with increasing c.

The concentration dependences of β_t and $\beta_{c,\nu}$ depend on the probe diameter. In many cases, there is a change in the concentration dependence near 3−4 g/L HPC. For most small ($d < 67$ nm) probes, β_t decreases almost linearly from 1 to 0.7−0.8, depending on d, as c rises from 0 to 7 g/L. For 67 nm probes, β_t decreases from 1.0 to 0.8 when c increases from 0 to 3−4 g/L, but β_t increases somewhat at higher polymer concentrations. $\beta_{c,\nu}$ is substantially scattered, but for $c > 3-4$ g/L $\beta_{c,\nu}$ generally declines (from 0.8 to 1.0 to 0.65−0.8) with increasing c. For 67 nm probes for $c > 3-4$ g/L, $\beta_{c,\nu}$ instead increases with increasing c. For most of small spheres for $c > 3-4$ g/L, $\beta_t \approx \beta_{c,0.55}$. For 14 nm spheres for $c > 3-4$ g/L, β_t is closer to $\beta_{c,0.5}$, while for $c < 3$ g/L, $\beta_{c,\nu}$ is too strongly scattered to identify β_t with a $\beta_{c,\nu}$. How are β_t, β_c, and β_η are related? For 14 nm spheres, $\beta_t \approx \beta_{c,0.5}$ is closely approximated by $\beta_{\eta,0.5}$ at all c. For 21, 38, and 67 nm spheres, and $c > 3-4$ g/L, $\beta_t \approx \beta_{c,0.55}$ exceeds even $\beta_{\eta,0.5}$. The concentration threshold 3−4 g/L at which β_t (for 67 nm spheres) and $\beta_{c,\nu}$ (for all spheres) change their behaviors is more than twice c^*. An equality $\beta_t \approx \beta_c$ at $c > 2c^*$ and a less satisfactory degree of equality between β_t and β_c at $c < 2c^*$ is consistent with expectations of ref 32 that coupling/scaling is more likely to be valid in nondilute solution. For small probes in polymer solution, because $\beta_t \approx \beta_c$ we may say that a single coupling coefficient n_D characterizes both the time and concentration dependences of $g^{(1)}(t)$.

The inequality between β_η and β_t for $c > 2c^*$ for small spheres is a coupling/scaling prediction. β_η describes relaxations of whole chains; β_t and β_c describe probe motions.[21] Under the coupling model,[32] increasing the strength of dynamic constraints increases the coupling coefficient n. Whole polymer chain motions encounter larger dynamic constraints than do small probe motions, because viscous flow moves whole chains. Small probe diffusion is coupled less strongly to chain motion than viscosity is coupled to chain motion, because small probes ($d \leq R_g$) can translate while displacing only part of each neighboring chain. The viscosity coupling coefficient $n_\eta = 1 - \beta_\eta$ is, therefore, expected to be larger than the probe coupling coefficient n_D, implying $\beta_\eta < \beta_t \approx \beta_c$, as found experimentally for 21, 38, and 67 nm probes for $c > 3-4$ g/L. The only exception to this predicted behavior involves the 14 nm spheres, where, for $c > 3-4$ g/L, $\beta_{\eta,0.5} \approx \beta_t$. This deviation from the expected behavior can probably be explained by noise in the data on 14 nm spheres. The fitting parameters θ and β are much more strongly scattered for 14 nm spheres than for other small spheres, but even for 14 nm spheres $\beta_{\eta,\nu} < \beta_{c,\nu}$ and $\beta_{\eta,0.55} < \beta_{c,0.55} \approx \beta_t$, as predicted.

In summary, for the slow mode of small spheres there are extensive areas of agreement between the data of ref 21 and coupling model predictions for β_η, β_t, and β_c. The prediction $\beta_c > \beta_\eta$ implies that $\theta\eta$ depends on c, because θ has the same dependence on β_c that η^{-1} has on β_η, β_c and β_η both depend on c, and $\beta_c \neq \beta_\eta$. Reference 21 indeed found for small spheres that $\theta\eta$ increases with increasing c, as expected from the relationship $\beta_c > \beta_\eta$. Equivalently, the non-pseudo-Stokes−Einsteinian behavior ($\theta\eta$ not a constant) for small probes, observed by ref 21, implies $\beta_c \neq \beta_\eta$.

Figure 2 gives exemplary results for the slow mode of large 455 nm probes; similar results are found for 87, 189, and 282 nm probes. For large spheres, $\beta = 1$. β_c and β_η are both substantially less than β_t. For the slow mode of large spheres, coupling/scaling predictions are not correct.

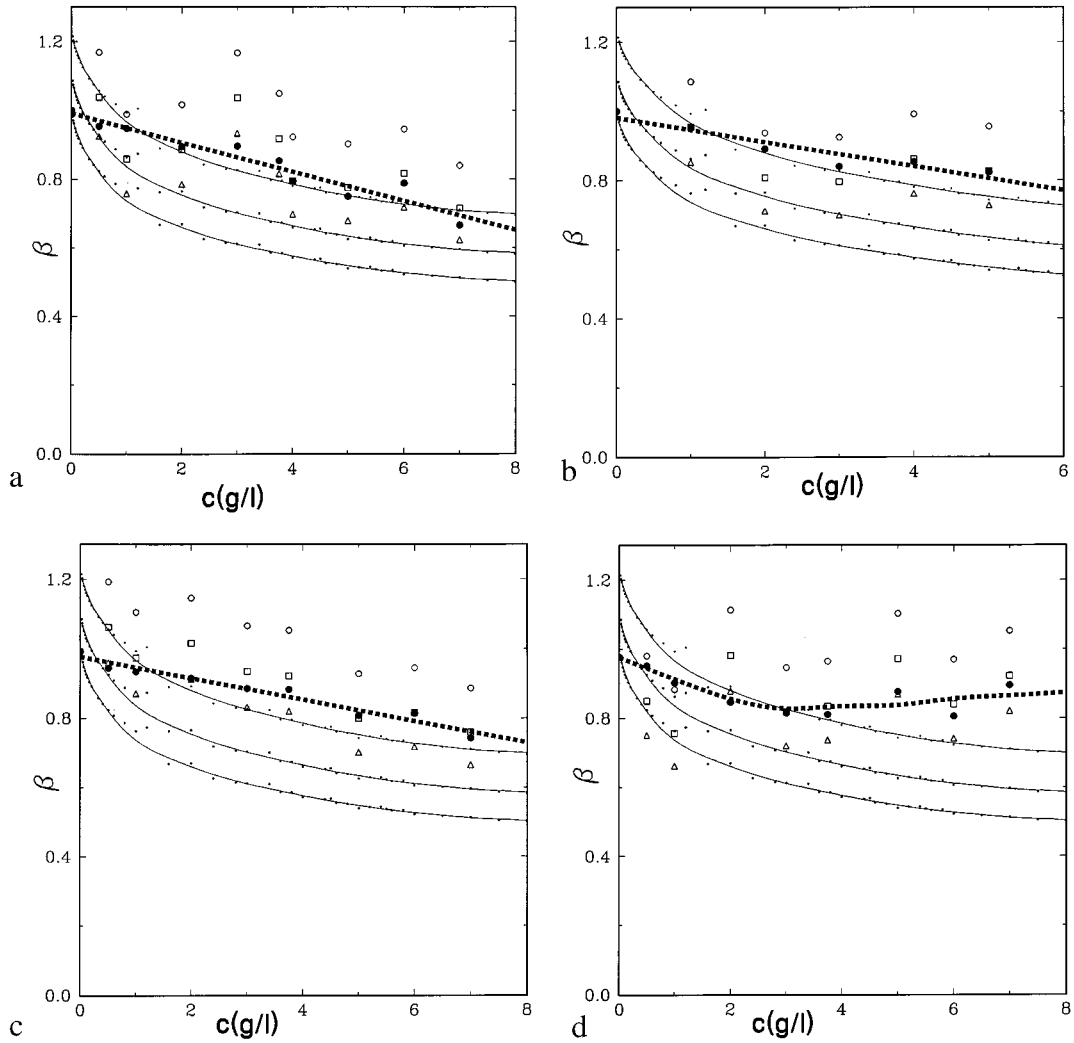

Figure 1. Slow mode exponents: (1) β_t from $g^{(1)}(t)$[21] via eq 4 (filled circles); (2) β_c from θ via eq 12 (open symbols corresponding, top-to-bottom, to ν of 0.5, 0.55, and 0.6) for small probes of diameter (a) 14, (b) 21, (c) 38, and (d) 67 nm in solutions of 1 MDa HPC; (3) β_η (small dots) from η[10] via eq 14. Solid lines are guides for the eye; they correspond to $\beta_{\eta,\nu}$ with ν of (top-to-bottom) to 0.5, 0.55, and 0.6. The dashed line, drawn to guide the eye, corresponds to $\beta_c(c)$.

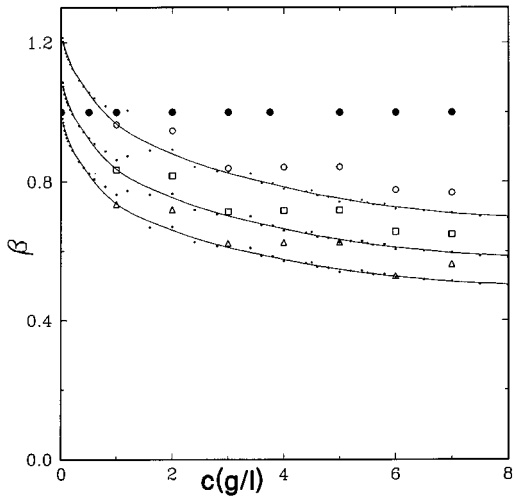

Figure 2. Slow mode exponents: (1) $\beta_t = 1$ from $g^{(1)}(t)$[21] via eq 4 (filled circles); (2) β_c from θ via eq 12 (open symbols corresponding, top-to-bottom, to ν of 0.5, 0.55, and 0.6) for large 455 nm probes in 1 MDa HPC solutions; (3) β_η (small dots) from η[10] via eq 14. Lines are the same as Figure 1.

For large probes, the parameters β_c and β_η both decrease with increasing c, β_c by ~0.3 over the concentration range studied. The difference between $\beta_{c,\nu}$ and $\beta_{\eta,\nu}$ decreases on increasing the probe diameter from 87 to 455 nm. In ref 21 the larger probes showed better agreement with pseudo-Stokes−Einsteinian behavior; for 189, 282, and 455 nm spheres $\theta\eta$ is constant to within a factor of 2. From the point of view of the coupling/scaling model, the functional dependences of β_c on θ and β_η on η^{-1} are the same. Since for large spheres θ and η^{-1} have approximately the same concentration dependence, the observed $\beta_c \approx \beta_\eta$ is to be expected. The 87 nm spheres did not show[21] pseudo-Stokes−Einsteinian behavior, so for these probes $\beta_c \neq \beta_\eta$ as expected.

We also examined β_τ, from τ, for the slow mode of small spheres (Figure 1a−d, Supporting Information). For $d < 67$ nm, $\beta_{c,0.5} = \beta_t < \beta_{\tau,\nu}$ at any ν. For 67 nm spheres, $\beta_{c,\nu} \approx \beta_{\tau,\nu}$. If the coupling/scaling model referred to τ rather than θ, one would expect $\beta_{c,\nu} = \beta_{\tau,\nu}$ for some ν. For large spheres, $\beta \equiv 1$ so $\tau = \theta^{-1}$; for large spheres the concentration dependences of β_c and β_τ are the same.

Coupling/Scaling Analysis of the Fast Mode

We now consider the fast mode. Reference 21 found that the fast mode is a stretched exponential $\exp(-\theta_f t^{\beta_f})$ that θ_f does not scale as q^2 and that β_f decreases with increasing c and inferred that the fast mode involves coupling to polymer internal modes.

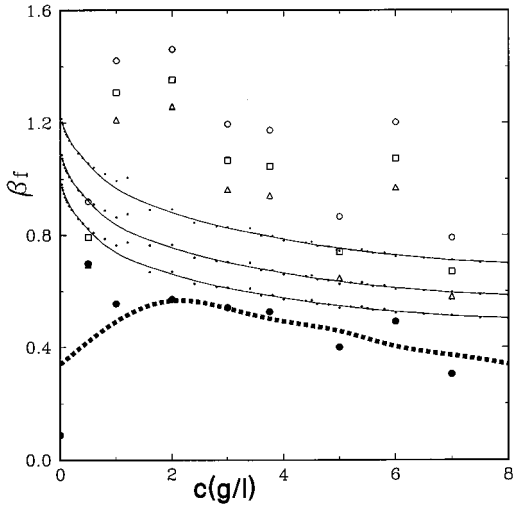

Figure 3. Fast mode exponents: (1) β_{ft} from $g^{(1)}(t)$[21] via eq 4 (filled circles); (2) β_{fc} from θ_f via eq 12 (open symbols, corresponding, top-to-bottom, to ν of 0.5, 0.55, and 0.6) for small 38 nm probes in 1 MDa HPC solutions; (3) β_η (small dots) from η[10] via eq 14. Solid lines are the same as Figure 1. The dashed line, drawn to guide the eye, corresponds to $\beta_{fc}(c)$.

Figures 3 and 4 compare the stretching exponents β_{ft}, β_{fc}, and β_η. Figure 3 shows exemplary results for β_f for small spheres ($d \leq 67$ nm); Figure 4a−e shows β_f for larger spheres ($d \leq 67$ nm). β_{fc} was obtained using eq 12 under the replacement $Dq^2 \rightarrow q_f$.

For probes with $d \leq 38$ nm (Figures 3), β_{ft} decreases with increasing concentration from ~0.6 to 0.2−0.3; β_{ft} is substantially less than β_η or β_{fc}. For 67 nm probes: β_{fc} is strongly scattered and c-independent below 4 g/L, and then decreases with rising c; β_{ft} approaches β_η at intermediate concentrations; $\beta_{fc,\nu}$ is usually larger than $\beta_{\eta,\nu}$. Just as $\beta_c > \beta_\eta$ usually obtained for the slow decay, so also is $\beta_{f,c}$ usually greater than β_η. Above 4 g/L, β_{fc} typically differs only 5−8% from β_c. While for the slow mode $\beta_t \approx \beta_c > \beta_\eta$, for the fast mode $\beta_{fc} > \beta_\eta > \beta_{ft}$. The inequality $\beta_{fc} < \beta_\eta$ corresponds to the failure of pseudo-Stokes−Einsteinian behavior for θ_f ($\theta_f\eta$ not constant), as shown in the previous section. The inequality $\beta_{fc} > \beta_{ft}$ does not agree with coupling/scaling prediction that independent estimates of β should agree. The coupling/scaling model thus fails for the fast mode of small probes.

Figure 4 plots β_f against c for large probes (67−455 nm). β_{ft} is consistently greater for large probes than for small probes; it generally decreases from 0.8 to 0.9 to 0.45−0.6 as c increases from 0 to 7 g/L. For probes with $d > 67$ nm $\beta_{fc,\nu}$ declines smoothly with increasing c; $\beta_{fc,\nu} \approx \beta_{\eta,\nu}$ at each ν. The concentration dependence of β_{ft} is slightly stronger than the concentration dependence of β_{fc} or β_η, so β_{ft} is closer to $\beta_{\eta,0.55}$ for $c < 4$ g/L but is closer to $\beta_{\eta,0.6}$ for $c > 4$ g/L. β_{ft} decreases weakly with probe diameter, so β_{ft} is closer to $\beta_{\eta,0.55}$ for 67, 87, and 189 nm probes and closer to $\beta_{\eta,0.6}$ for 282 and 455 nm probes. For 67 nm probes (Figure 4a) for $c \geq 3$ g/L, $\beta_{ft} \approx \beta_{\eta,0.55} \approx \beta_{fc,0.6}$. For larger probes ($d > 67$ nm) for $c \leq 4$ g/L, it is still approximately true that $\beta_{ft} \approx \beta_{fc,\nu} \approx \beta_{\eta,\nu}$ with $\nu = 0.55$ or $\nu = 0.6$, depending on c. The coupling/scaling model thus works well for the fast mode of large spheres.

We also calculated β_{τ_f} from τ_f^{-1} using eq 12 with $D \rightarrow \tau_f^{-1}$ (see Figure 2a−h, Supporting Information). For large probes and $c > 4$ g/L, $\beta_{\tau_f} \approx \beta_{\tau_f} \approx \beta_{f_c} \approx \beta_\eta$, so the above remarks on β_{fc} also apply to β_{τ_f}.

Discussion

Table 1 summarizes our results. For each mode and class of probes (large and small) the table shows the principal characteristics of the mode, viz.: (1) the order of magnitude and concentration dependence of θ or θ_f, (2) the relative values of β_t or β_{ft}, β_c or β_{fc}, and β_η, and (3) the success or lack thereof for the coupling/scaling model, based on the agreement with the prediction $\beta_t \approx \beta_c \approx \beta_\eta$. The coupling/scaling model works adequately for the fast mode of the large probes and the slow mode of small probes. Coupling/scaling fails for the other two mode/probe-size combinations.

We now advance two interpretations for the success or failure of the coupling/scaling model, namely an explanation based on the relationships between observed and assumed spectral line shapes, and an explanation based on the absolute time scale of the modes.

The first interpretation arises from the fundamental difference between the line shape presumed by the simple coupling model (which assumes that there is only one class of "basic units") and the line shape found experimentally. The simple coupling/scaling model predicts a single, stretched-exponential relaxation. Experimental data reveal a spectrum that is the sum of two stretched exponentials. Under the first interpretation, if one mode dominates a spectrum, and if the relaxation pseudorates θ and θ_f are not too different, then the experimental spectrum approaches the coupling-model form; in this case, we propose that the simple coupling/scaling model becomes applicable. Contrariwise, if the two observed modes have similar amplitude, or if θ and θ_f differ greatly from each other, then the observed spectra will differ markedly from the single-relaxation form of the simple coupling/scaling model. The simple coupling/scaling model does not describe a two-mode system, so it should not be applicable to both modes. However, it remains interesting to see if coupling/scaling describes either mode separately.

Our second interpretation for the applicability of the model is based on the assumption that probe relaxations reflect motions of polymer chains, and that, regardless of probe diameter, the chain behavior involves three physical time scales. On the shortest observed time scale, local motions of polymer chains are significant. The coupling model refers to the intermediate time scale. On the longest time scale, all polymer modes have decayed, so the solution behaves as a simple viscous fluid. The time scale on which probe motion is observed determines the time scale for the polymer motions that affects the probes.

To test the first interpretation, we examine seriatim the small and large spheres:

(i) *For small probes*,[21] $A_f \sim 0.2$, while $\theta_f/\theta = 5-10$. The slow mode dominates the spectrum and is only moderately separated from the fast mode. Under the first interpretation, the coupling/scaling model should describe the dominant slow mode but might or might not describe the secondary fast mode. For the slow mode, we find $\beta_t \approx \beta_{c,0.55}$ ($\beta_t \approx \beta_{c,0.5}$ for 14 nm spheres); for each ν, $\beta_{c,\nu}$ is greater than $\beta_{\eta,\nu}$. The slow mode is, therefore, consistent in part with the coupling/scaling expectation $\beta_\eta \approx \beta_c \approx \beta_t$. For the fast mode, one finds $\beta_{ft} < \beta_\eta$ and often $\beta_\eta < \beta_{fc}$, which is not consistent with the coupling/scaling model. The first interpretation thus correctly implies that coupling/scaling only applies to a dominant mode.

(ii) *For large probes*,[21] $A_f \sim 0.4-0.6$, while $\theta_f/\theta \geq 100$. The two modes have roughly equal amplitudes; the time scale separation of modes is much more pronounced than it was for small probes. Under the first interpretation, there is no reason for the coupling/scaling description to work for either mode, but it is of interest to see if the coupling/scaling model works

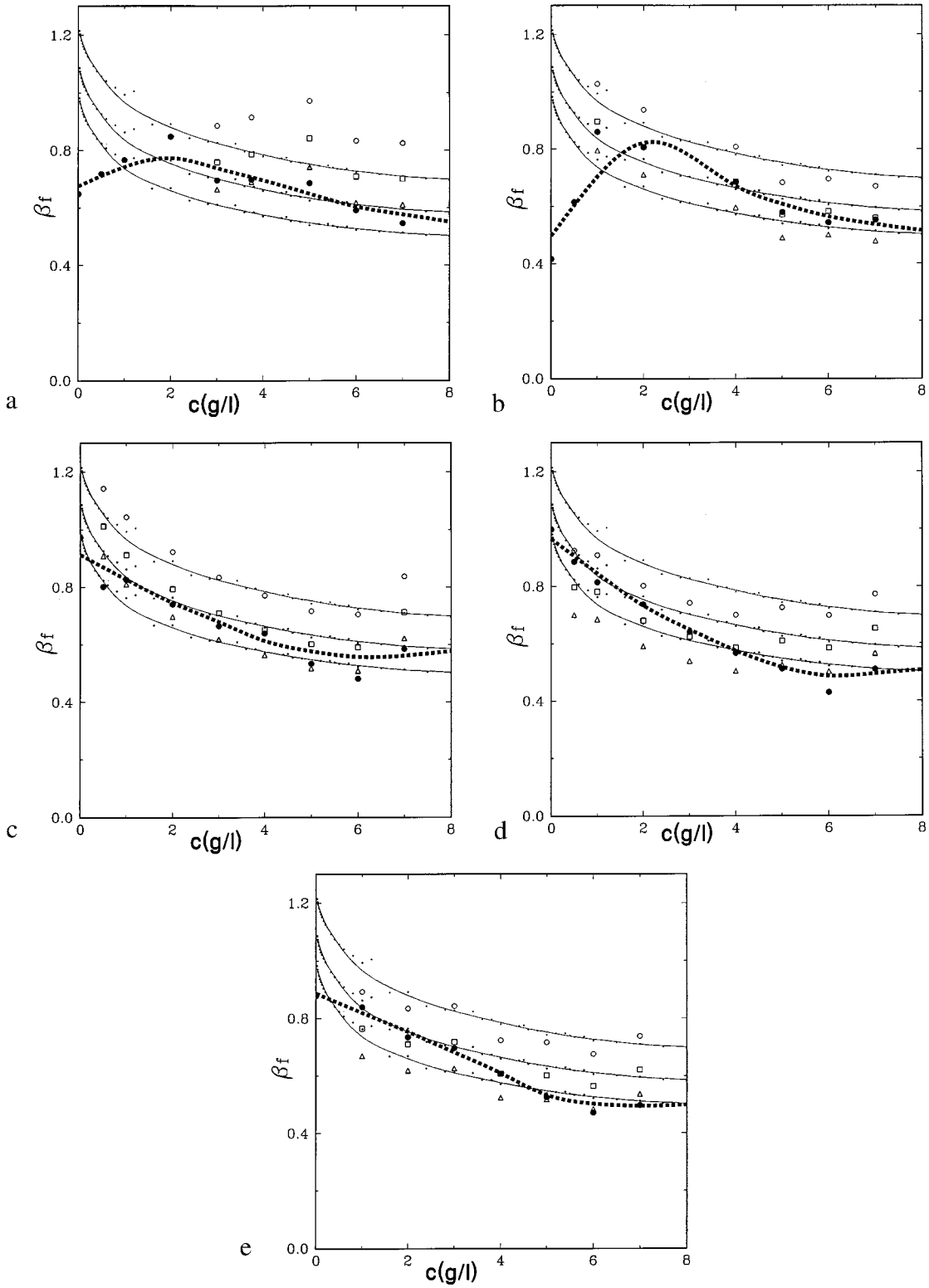

Figure 4. Fast mode exponents: (1) β_{ft} from $g^{(1)}(t)$[21] via eq 4 (filled circles); (2) β_{fc} from θ_f via eq 12 (open symbols, corresponding, top-to-bottom, to ν of 0.5, 0.55, and 0.6) for large probes of diameter (a) 67, (b) 87, (c) 189, (d) 282, and (e) 455 nm in solutions of 1 MDa HPC; (3) β_η from η[10] via eq 14 (small dots). Solid lines are the same as Figure 1. The dashed line, drawn to guide the eye, corresponds to $\beta_{fc}(c)$.

for either mode separately. For the slow mode, $\beta_\eta \leq \beta_c < \beta_t = 1$, contrary to the coupling/scaling prediction. The slow mode behavior is thus inconsistent with the coupling/scaling treatment but is consistent with the interpretation that coupling/scaling does not work if $g^{(1)}(t)$ does not approach a single stretched exponential. For the fast mode, the coupling/scaling prediction $\beta_{ft} \approx \beta_\eta \approx \beta_{fc}$ generally works, albeit with a weak dependence of optimal ν on sphere size, consistent with the suggestion that with a bimodal relaxation one should separately test each mode against coupling/scaling.

In summary, when one mode dominates, the coupling/scaling model works for the dominant mode. When two distinct modes are present, coupling/scaling works for one of the modes. The data of ref 21 are thus consistent with the first interpretation, namely that coupling/scaling treats a single dominant mode and may apply to one mode when several modes are present.

TABLE 1: Coupling/Scaling (c/s) Analysis of the Slow and Fast Modes of Large and Small Spheres[a]

	slow mode	fast mode
large probes ($d > R_g$)	$1 \equiv \beta_t > \beta_{c,\nu} \approx \beta_{\eta,\nu}$	$\beta_{ft} \approx \beta_{fc,\nu} \approx \beta_{\eta,\nu}$
	$\theta \sim 10^{-3}$ to 5×10^{-6}	$\theta_f \sim 10^{-2}$ to 3×10^{-3}
	$\theta \sim \exp(-\alpha c^{\nu})$	$\theta_f \sim c^0$
	$d\tau/dc > 0$	$d\tau_f/dc > 0$
	c/s fails	c/s successful
small probes ($d < R_h$)	$\beta_t \approx \beta_{c,0.55} \geq \beta_{\eta,0.55}$	$\beta_{ft} \leq \beta_{\eta,\nu} \leq \beta_{fc,\nu}$
	$\theta \sim 10^{-2}$ to 3×10^{-3}	$\theta_f \sim 5 \times 10^{-2}$
	$\theta \sim c^0$	$\theta_f \sim c^0$
	$d\tau/dc > 0$	$\tau_f \sim c^0$
	c/s largely successful	c/s fails

[a] θ_i and β_i are defined in the text.

We now consider the second interpretation for the success or failure of coupling/scaling. In this interpretation, the character of probe relaxations on a time scale is determined by the polymer relaxations on the same time scale. Mode properties are thus controlled by the mode's absolute time scale. From Table 1, our probe relaxations have three time scales, namely: (1) the large-probe slow mode with $\theta \sim 10^{-3}$ to 5×10^{-6}, (2) the large-probe fast mode and the small-probe slow mode with θ_f or $\theta \sim 1 \times 10^{-2}$ to 3×10^{-3}, and (3) the small-probe fast mode with $\theta_f \sim 5 \times 10^{-2}$.

Mode time scales may also be characterized by τ and τ_f, eq 5. θ and τ have different dimensions, so they are inequivalent. For four mode/probe-size combinations τ and τ_f are (i) $\tau \sim 10^{-3}$ to 3×10^{-1} s for the large-probe slow mode, (ii) $\tau_f \sim 6 \times 10^{-4}$ to 10^{-1} s for the large-probe fast mode, (iii) $\tau \sim 10^{-4}$ to 8×10^{-4} s for the small-probe slow mode, and (iv) $\tau_f \sim 3 \times 10^{-4}$ to 5×10^{-2} s for the small-probe fast mode. While only θ (and not θ_f) is strongly concentration dependent, and then only for large probes, τ increases with increasing c for all probes, and τ_f also increases for large but not small probes. The ranges of τ and τ_f appear to overlap, but comparing large and small probes at every concentration: $\tau^{large} > \tau_f^{large} > \tau^{small}$.

The longest time scale involves the large-probe slow mode, which has the largest τ. We can rationally incorporate the large-probe fast mode (τ_f^{large}) and the small-probe slow mode (τ^{small}) into a single intermediate time scale. The small-probe fast mode, while strongly scattered, usually satisfies $\tau_f^{large} \geq \tau_f^{small} \geq \tau^{small}$; i.e., for small probes $\tau_f > \tau$ even though $\theta_f > \theta$. However, $\beta \approx 0.5-0.9 > \beta_f \approx 0.2-0.5$, so the small-probe fast mode has a very sharp initial decay. It is therefore rational to label the small-probe (θ_f, β_f)-mode as the "fast" process, even though $\tau_f^{small} \geq \tau^{small}$. In terms of a three-time-scale description of the system, the large-probe slow mode describes a time scale so long that polymer:solvent internal modes have completely relaxed. To the probes the medium is very nearly a simple viscous fluid. The central limit theorem then ensures that probes perform simple Brownian motion, implying $\beta_t = 1$ and $\theta \sim q^2$, as found experimentally. Phenomenologically, both θ and η depend on c via $\exp(-\alpha c^{\nu})$, while $\theta\eta$ is nearly independent of c (simple Stokes−Einsteinian behavior at long times), so $\beta_{c,\nu} \approx \beta_{\eta,\nu}$.

The fast mode of large probes and the slow mode of small probes have a variety of similar features, besides their common time scale; in particular, they have similar concentration dependences for their decay pseudorates and stretching exponents.

Figure 5 shows τ (small probes) and τ_f (large probes). Both τ and τ_f increase with rising c. The concentration dependence of the large-probe τ_f is stronger than the concentration dependence of the small-probe τ, consistent with the expectation that larger probes couple more strongly to polymer motions than

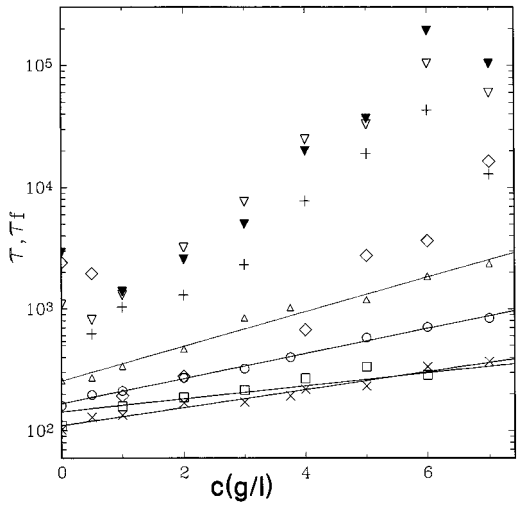

Figure 5. Concentration dependences of the decay times $\tau = \theta^{-1/\beta}$ for the slow mode of small probes with diameter 14 (X), 21 (□), 38 (○), and 67 (△) nm and of the decay times $\tau_f = \theta_f^{-1/\beta_f}$ for the fast mode of large spheres with diameter 87 (◇), 189 (+), 282 (▽), and 455 (▼) nm. Units of τ and τ_f are μS.

do small probes. However, the decay pseudorates θ and θ_f are concentration-independent; τ and τ_f inherit their dependences on c from β and β_f exclusively.

We identify these two modes with the intermediate time scale. The relaxation on this scale is correctly described by the coupling/scaling model. Experimental phenomenology supportive of this interpretation includes (i) the observed line shape is a stretched-exponential in t, (ii) β (small spheres) and β_f (large spheres) fall with increasing c, consistent with the coupling model expectation that the coupling coefficient n increases (and hence $\beta = 1 - n$ decreases) with increasing c, (iii) both modes largely comply with the coupling/scaling prediction $\beta_t = \beta_c = \beta_\eta$, namely for large spheres $\beta_{ft} \approx \beta_{fc,\nu} \approx \beta_{\eta,\nu}$, while for small spheres $\beta_t \approx \beta_{c,\nu}$ (though β_t, $\beta_{c,\nu} > \beta_{\eta,\nu}$), and (iv) a mode with strong coupling to polymer relaxations should have a concentration-dependent relaxation rate; indeed, τ (small probes) and τ_f (large probes) depend on c. All things considered, the phenomenology thus supports our identification of the intermediate time scale mode as the mode that follows the coupling/scaling model.

At very short times, coupling has not fully established itself. This time scale is sampled by the fast-mode motions of small probes. This short-time mode is not the same as the early-time regime of the Ngai model, which has a simple-exponential relaxation. Small probes are much smaller than chains, so a small probe is unlikely to be in contact with more than one or two chains at a time. Chain interactions have not yet fully established themselves, so θ_f should be relatively independent of c, as observed experimentally. If probe motions are dominated by the motions of one neighboring chain, θ_f will be determined by internal chain dynamics and will be relatively independent of d, also as observed experimentally. Finally, in a mode in which coupling is not yet fully asserted, n_f for that mode will be less than n_η for bulk flow, implying β_{ft}, $\beta_{fc} > \beta_\eta$, as observed experimentally for the small-probe fast mode.

The evidence for the second interpretation of Table 1 is not totally unambiguous. Consider the modes to which coupling/scaling was said to apply. For the fast mode of large probes $\beta_{fc} \approx \beta_{ft} \approx \beta_\eta$, but for the slow mode of small probes β_c, $\beta_t > \beta_\eta$, which is not the coupling/scaling prediction. The difference between large and small-probe intermediate-time-scale relaxations may be rationalized in terms of probe diameter. For large probes, A_f is largely independent of q^2; large probes are fully

coupled to solvent motions on all distance scales. For small probes, A_f depends strongly on q^2. Probes with $d < 2R_g$ are small enough to be sensitive to solution structure, not just to the long-wavelength shear viscosity of the medium. While coupling coefficients for large-probe motion agree with β_η (n_η), the coupling coefficients for small-probe slow motion are mutually consistent, but differ from the viscosity coupling coefficient. However, larger probes should experience stronger dynamic constraints than do the smaller probes. Therefore, according to coupling/scaling, the coupling coefficient n_{large} of large probes should be larger than the coupling coefficient n_{small} of small probes, implying $\beta_{ft,large} < \beta_{t,small}$, as found experimentally.

Ngai and Phillies[32] showed that Phillies and Lacroix's[20] recent measurements of probe diffusion in 300 kDa HPC are consistent with coupling/scaling predictions. The line shapes reported by Phillies and Lacroix[20] are superficially different from those we reported in ref 21. Phillies and Lacroix generally found a single stretched exponential spectrum, with a weak ($\leq$4% of the amplitude) very fast exponential mode being seen at elevated polymer concentrations. In contrast, as described above, we[21] reported bimodal spectra for probes in 1 MDa HPC solutions. The difference in line shape descriptions apparently arises because spectra in ref 20 typically were measured over 1.5 or 2 decades of decay, while spectra in ref 21 typically covered 2+ to 3 decades of decay. To confirm that the line shape descriptions for probes in solutions of 300 kDa and 1 MDa would agree if all spectra were measured out to the same $S(q,t)/S(q,0)$, we made[22] additional measurements on probes in 300 kDa HPC solutions, measuring spectra out to $S(q,t)/S(q,0) \approx 1 \times 10^{-3}$. With small probes in 300 kDa HPC, we found[22] an additional weak ($A_f \sim 0.08-0.15$) fast stretched-exponential mode; with large probes, we identified[22] an additional slow, pure-exponential mode.

Taking these additional modes into account, the observed probe modes in 300 kDa HPC correspond exactly in all their properties to the modes seen in Table 1 and ref 21. Our new data[22] on probes in 300 kDa HPC show that probe spectra have the same functional form with either molecular weight of polymer. Furthermore, the spectral modes that were characterized in ref 20 and found in ref 32 to follow coupling/scaling are shown by our new measurements[22] to be the small-probe slow mode and the large-probe fast modes, these being the modes shown above to follow coupling/scaling in 1 MDa HPC solutions. Regardless of the molecular weight of the HPC, it is the intermediate-time-scale mode whose parameters follow coupling/scaling. In particular, the intermediate-time-scale mode of both 300 kDa[20,22] and 1 MDa HPC[21] has the following features characteristic of coupling/scaling: (i) $g^{(1)}(q,t)$ is a stretched exponential, (ii) β (small spheres) and β_f (large spheres) both fall with increasing c, (iii) $\beta_t \approx \beta_c \approx \beta_\eta$ for small spheres, and $\beta_{ft} \approx \beta_{fc} \approx \beta_\eta$ for large spheres, and (iv) τ and τ_s both increase with rising c. Furthermore, for both polymers the intermediate-time-scale mode shows yet another common physical property: $\tau/\eta \neq$ constant for small spheres, but $\tau_f/\eta \approx$ constant for large spheres. (See Figure 3a,b of Supporting Information for $\tau/\eta(c)$ for small probes and $\tau_f/\eta(c)$ for large probes in 1 MDa HPC[21]. Both the small-probe slow mode and the large-probe fast mode in 1 MDa and in 300 kDa HPC, therefore, not only comply with the coupling/scaling model but also have other similarities in their physical properties.

The most prominent dependence of spectral line shape on the polymer molecular weight is that for small probes in 300 kDa HPC, $\beta_t \approx \beta_c \approx \beta_\eta$, while for some probes in 1 MDa HPC, $\beta_t \approx \beta_{c,0.55} \geq \beta_{\eta,0.55}$. Because the spectral features are substantially independent of polymer M, our interpretations as to why coupling/scaling succeeds or fails are equally applicable at either M.

In conclusion, we used the coupling/scaling model of Ngai and Phillies[32] to analyze QELSS spectra of probes in 1 MDa HPC.[21] The coupling/scaling model does not predict the observed bimodal spectra but works for some individual spectral modes; namely, it describes the large-probe fast mode and the small-probe slow mode. Two interpretations for this success of the coupling/scaling model were advanced, based on the observed line shapes and on the observed time scales. For small probes, coupling/scaling describes the dominant mode, as argued by our first interpretation. For large probes, coupling/scaling works for the fast mode but not the slow mode. The coupling/scaling model succeeds for the modes that appear to involve coupling to the chain internal motions. In the second interpretation, coupling/scaling works on an intermediate-time-scale (where probe motions are coupled to polymer relaxations), but not on the long time scale (where all polymer modes have relaxed so probes move as in a simple viscous fluid) or the very short time scale (where coupling is not yet established). Finally, our new data on 300 kDa HPC[22] demonstrate that our findings on the success or failure of the coupling/scaling model for probes in 1 MDa HPC are consistent with the earlier coupling/scaling analysis of probes in 300 kDa HPC.[20,22,32]

Acknowledgment. The partial support of this work by the National Science Foundation under Grant DMR94-23702 is gratefully acknowledged.

Supporting Information Available: Plots of β_τ, computed from concentration dependence of τ, for the slow mode of small probes. Plots of β_{τ_f}, computed from concentration dependence of τ_f, for the fast modes of small and large probes. Plots of τ/η for all probes and τ_f/η for large probes (14 pages). This information is available free of charge via the Internet at http://pubs.acs.org.

References and Notes

(1) Doi, M.; Edwards, S. F. *The Theory of Polymer Dynamics*; Oxford University Press: Oxford, U.K., 1986.
(2) de Gennes, P. G. *Scaling Concepts in Polymer Physics*; Cornell University Press: Ithaca: NY, 1979.
(3) Phillies, G. D. J. *J. Phys. Chem.* **1989**, *93*, 5029.
(4) Ngai, K. L.; Rajagopal, A. K.; Teiler, S. *J. Chem. Phys.* **1988**, *88*, 5086.
(5) Phillies, G. D. J. *J. Phys. Chem.* **1992**, *96*, 10061.
(6) Nystrom, B.; Roots, J.; Carlsson, A.; Lindman B. *Polymer* **1992**, *33*, 2875.
(7) Bu, Z.; Russo, P. S. *Macromolecules* **1994**, *27*, 1187.
(8) Furukawa, R.; Arauz-Lara, J. L.; Ware, B. R. *Macromolecules* **1991**, *24*, 599.
(9) Phillies, G. D. J. *Macromolecules* **1995**, *28*, 8198.
(10) Phillies, G. D. J.; Quinlan, C. *Macromolecules* **1995**, *28*, 160.
(11) Phillies, G. D. J.; Richardson, C.; Quinlan, C. A.; Ren, S.-Z. *Macromolecules* **1993**, *26*, 6849.
(12) Phillies, G. D. J.; Clomenil, D. *Macromolecules* **1993**, *26*, 167.
(13) Nystrom, B.; Lindman, B. *Macromolecules* **1995**, *28*, 967
(14) Camins, B.; Russo, P. S. *Langmuir* **1994**, *10*, 4053.
(15) Kjoniksen, A.-L.; Nystrom, B. *Macromolecules* **1996**, *29*, 7116.
(16) Ren, S. Z.; Shi, W.; Zhang, W.; Sorensen, C. M. *Phys. Rev. A* **1992**, *45*, 2416.
(17) Ren, S. Z.; Sorensen, C. M. *Phys. Rev. A* **1993**, *11*, 1727.
(18) Nystrom, B.; Thuresson, K.; Lindman, B. *Langmuir* **1995**, *11*, 1994.
(19) Brown, W.; Nicolai, T. *Macromolecules* **1994**, *27*, 2470.
(20) Phillies, G. D. J.; Lacroix, M. *J. Phys. Chem. B* **1997**, *101*, 39.
(21) Streletzky, K. A.; Phillies, G. D. J. *J. Chem. Phys.* **1998**, *108*, 2975.

(22) Streletzky, K. A.; Phillies, G. D. J. Probe Diffusion in Hydroxypropylcellulose-Water Solution. Effect of Polymer Molecular Weight. Manuscript in preparation.
(23) Cicerone, M. T.; Blackburn, F. R.; Ediger, M. D. *Macromolecules* **1995**, *28*, 8224.
(24) Walderhaug, H.; Nystrom, B.; Hansen, F. K.; Lindman, B. *J. Phys. Chem.* **1995**, *99*, 4672.
(25) Ngai, K. L.; Rendell, R. W. *J. Mol. Liq.* **1993**, *56*, 199.
(26) Ngai, K. L.; Rendell, R. W.; Rajagopal, A. K.; Teiler, S. *Ann. N. Y. Acad. Sci.* **1985**, *484*, 150.
(27) Rizos, A. K.; Jian, T.; Ngai, K. L. *Macromolecules* **1995**, *28*, 517.
(28) Nystrom, B.; Walderhaug, H.; Hansen, F. K. *J. Phys. Chem.* **1993**, *97*, 7743.
(29) Ngai, K. L.; Wang, Y.-N.; Magalas, L. B. *J. Alloys and Compounds* **1994**, *211/212*, 327.
(30) A recent review: Ngai, K. L. In *Disorder Effects in Relaxational Processes*; Richert, R., Blumen, A., Eds.; Springer: Berlin, 1994; pp 89−150.
(31) Phillies, G. D. J.; Ullmann, G. S.; Ullmann, K.; Lin T.-H. *J. Chem. Phys.* **1985**, *82*, 5242.
(32) Ngai, K. L.; Phillies, G. D. J. *J. Chem. Phys.* **1996**, *105*, 8385.
(33) Brown, W.; Rymden, R. *Macromolecules* **1986**, *19*, 2942.
(34) Mustafa, M. B.; Russo, P. S. *J. Colloid Interface Sci.* **1989**, *129*, 240.
(35) Tsang, K. Y.; Ngai, K. L. *Phys. Rev. E* **1996**, *54*, R3067.
(36) Tsang, K. Y.; Ngai, K. L. *Phys. Rev. E* **1997**, *56*, R17.